SPE 9328

SPE

A CONSTITUTIVE EQUATION FOR NONLINEAR STRESS-STRAIN CURVES IN ROCKS AND ITS APPLICATION TO STRESS ANALYSIS AROUND A BOREHOLE DURING DRILLING

by Nobuo Morita and K.E. Gray, University of Texas

ABSTRACT

The stress-strain behavior of Berea, Ohio, and Pecos sandstone was measured intensively under triaxial loading paths. Both compression and extension tests were performed at different pore fluid pressures. These tests showed that four modes can arise in the stress-strain curves up to failure: an initial nonlinear portion; linear portion; a final nonlinear portion; and volume change of the rock maxtrix due to pore fluid pressure. The characteristics of these modes were studied,and a nonlinear model was developed to represent the important characteristics, i.e., the four modes, of the behavior of sandstones by means of a constitutive equation in such a way as to satisfy certain mathematical requirements.

A finite element model using nonlinear stress-strain relationship was developed which simulates the stress state of a structure up to failure. The finite element model was used to predict fracture pressure around a borehole during drilling. The shape of the borehole is either circular or elliptic, and the tectonic stress is directional. Since the nonlinear stress state depends upon loading history, the loads were applied incrementally, simulating phenomena occuring during the drilling process. It is shown that use of conventional linear stress-strain behavior gives significantly erroneous results for well stability problems.

INTRODUCTION

The finite element method has now become recognized as a general method of wide applicability to engineering and physical science problems. As a result of its broad applicability and systemactic generality, the method has gained wide acceptance by civil engineers and architectural engineers for designing rock structures and soil foundations.

Experimental studies[7] on rock and soil behavior have been conducted since the early 20th century. Numerous data of the effect of temperature, pore pressure, stress state and time upon rock and soil behavior have been published. In the 1960's, various simple nonlinear constitutive equations [8,9] were proposed. Although these were helpful for analytical use, the development of sophisticated numerical discretization techniques need not require simplified constitutive equations.

References and illustrations at end of paper.

Most nonlinear equations were developed in the past to fit nonlinear stress-strains for metals and soils. Consequently, one often encounters trouble applying them to porous materials consisting of grains. Rock exhibits volumetric expansion and compression and also increased rigidity as hydrostatic pressure increases. For instance, the nonlinearity of sandstones is significant in radial strain rather than axial strain for triaxial compression tests. This is due to volumetric expansion caused by the sliding between grains before failure of rock occurs. Since the rigidity increases with hydrostatic pressure, the usual deviatoric stress-strain relations can not be applied to sandstones. Various nonlinear constitutive stress-strain relationships were tested by the present authors before this work was initiated. These include equations proposed by Barla,[1] Drucker,[5,6] Von Mises[8], Prandtle[9], Mroz[12] and Dienes[4]. But none of them could simultaneously take into account nonlinear volumetric change and increased rigidity due to hydrostatic pressure for both compression and extension. Although the nonlinear equations proposed by Sandler[13] and Prevost[11] partially satisfy these requirements, they do not represent accurately both axial and radial stress-strain of sandstones with pore pressure under triaxial extension and compression loading. In this work, the nonlinear constitutive equation was assumed to be composed of four parts: an initial nonlinear part, an elastic part, a plastic part, and volume change of the rock matrix due to fluid pressure. Each part was carefully examined and expressed by mathematically consistent equations. Thus, a nonlinear constitutive equation was established which closely simulates the nonlinear behavior of sandstones with pore pressure and was applied to a finite element simulator.

Estimation of fracture gradient is important for the drilling operation since it limits the maximum density of the drilling fluid. It also gives the maximum borehole strength at the casing shoe during kick control operations. Estimation of the fracture gradient is erroneous if one simply applies the linear stress-strain behavior. The stress state changes on a wide range before borehole rupture, including significant nonlineality in stress-strain relations for the rock. In this work, the fracture gradient around a wellbore was studied, as an example of the practical application of the finite element model using nonlinear stress-strain. The minimum fracture gradient usually occurs when the surface of the wellbore cracked or notched. In this case the fracture gradient is close to the tectonic stress gradient. On the other hand,

when the wellbore surface is smooth, higher gradients can be observed. This higher pressure was calculated for a wellbore with mud cake to study the effect of the directional tectonic stress and an elliptic wellbore.

STRESS-STRAIN BEHAVIOR OF SANDSTONES

Experimental Procedures

Three sandstones(Berea, Ohio, and Pecos) were used in this study. Indiana limestone was used only for measuring the effective stress constant under static conditions. These rocks were selected because they are frequently used as test materials for rock mechanics research conducted in North America and because their permeability are widely different (180 to 400 md for Berea sandstone, 6 md for Ohio sandstone, and 0.2 md for Pecos sandstone). Porosities were around 20.7 percent for Berea sandstone, 19.5 percent for Ohio sandstone and 18.1 percent for Pecos sandstone. The effective stress constant was measured for Indiana limestone because it is significantly different from the value of one reported in previous works.[7,12] Specimen length was approximately 3.8 in. for Ohio sandstone and 4.5 for Indiana limestone, Pecos and Berea sandstone. Specimen diameter was 1.985 in.. Berea sandstone and Ohio sandstone samples were saturated with water. Pecos sandstone and Indiana sandstone were used dry. After the specimen was mounted in the pressure cell, an appropriate confining pressure and pore pressure were applied to the core. The specimen was then made to fail in either compression or extension by moving the platen of an MTS machine at a constant loading rate of .1 Kpsi/sec in compression or .02Kpsi/sec in extension. For measurement of the rock matrix, both the pore pressure and the confining pressure were increased simultaneously up to an appropriate pressure and decreased to zero. After that, the bulk modulus of the specimen was measured increasing only the confining pressure.

Profile of the stress-strain curves

Figs. 1 to 6 show stress-strain data for Berea sandstone up to maximum strength. For compression tests, two types of nonlinearity (Figs. 7) were found in the initial and final portions of the stress-strain curves, separated by straight portion. The initial nonlinearity is compressive and pertains only to the direction in which the load is applied. The directional behavior is large perpendicular to the bedding planes. On the other hand, the final nonlinearity is not compressive but the volume of the rock significantly increases with loading up to failure. Particularly significant nonlinearity appears in the circumferential strain. The straight portion between these nonlinearities does not show much anisotropy, and the slope approaches a constant with higher confining pressure.

For extension tests, a straight portion appears when the rock specimen is extended after being compressed hydrostatically. It is followed by a nonlinear portion where the nonlinearity of the circumferential strain is trivial compared with the axial strain.

Physically, these experimental phenomena may be explained as follows. The sandstone generally consists of solid grains, loose material such as clay, and pore capillaries surrounded by many flat cracks. If it is compressed, the flat cracks around pore capillaries start closing. Due to variation in the ratio of the major and minor axes and in their direction of the penny shaped cracks, the stress-strain curve exhibits nonlinearity approaching exponentially to a constant value until all the flat cracks close. The

displacement of the crack surface is trivial if it is compressed in the direction of the major axis of the penny shaped cracks but nontrivial in the direction of the minor axis. Accordingly, the penny shaped cracks lying in the direction approximately perpendicular to the loading respond to the load, which causes large strain parallel to the load but trivial strain perpendicular to it.

After most of the cracks, whose major axis is perpendicular to the load, are closed, a linear stress-strain relation appears. For sufficiently high confining pressure, the slope is approximately independent of the confining pressure because, for this range of stress state, no dislocation occurs in the rock. In other words, the rock consisting of rock material and pore capillaries deforms without pore closing or micro fracture growth.

The final nonlinearity which follows the continuous linear deformation may be attributed to the growth of micro cracks during onset of failure. The volume of the rock increases significantly for small confining pressure. For large confining pressure, the volume change is not significant and the rock behaves as an ideally plastic material.

Effect of Confining Pressure

The effect of confining pressure on stress-strain is shown in Figs. 1 and 2 for confining pressure up to 11 Kpsi. For Berea sandstone the slopes of the straight portion of σ_z vs ε_z and σ_z vs ε_θ increases up to P_c=3Kpsi but become approximately constant for higher confining pressure. The same behavior was noted for Ohio sandstone. However, for Pecos sandstone, the slopes remain approximately constant for any confining pressure. The Young's modulus and Poisson's ratio approach approximately $3.7x10^3$ Kpsi and 0.14 for Berea sandstone, $2.85x10^3$ Kpsi and 0.16 for Ohio sandstone and $2.9x10^3$ Kpsi and 0.14 for Pecos sandstone, respectively, with higher confining pressure.

Initial nonlinearity in the stress-strain curves was significant only for P_c=0, 1 and 3 Kpsi for Berea (Figs. 1 and 2) and Ohio sandstones. If the rock specimen is loaded hydrostatically (Fig.3), the volume of rock is nonlinearly reduced due to closing of flat cracks surrounding pore capillaries. Since more cracks are oriented along the bedding planes, the strain perpendicular to them is larger than the parallel case. For Pecos sandstone the stress-strain curves are straight and almost identical for both σ_z vs ε_z and σ_z vs ε_θ. This sandstone is quite tight and fewer open flat cracks may exist around pore capillaries.

Due to the various orientations of the cracks and the ratios of the major and minor axes of penny shaped cracks, opening and closing of the cracks depends upon the stress level. Fig.7 shows the phenomenon schematically. For compression, the nonlinear strain, ε_{ii}^N, due to crack opening and closing exponentially approaches a straight line parallel to AB. For smaller stress levels, the cracks flatter and lying closer to the direction perpendicular to the load are closing, and for larger stress levels, those more circular and lying not in the direction still remain open and are closing. For tension, they keep opening until fine cracks start developing from the edge of the original cracks. In order to treat the phenomenon quantitatively, $\log[(a_i-\varepsilon_{ii}^N)]$ vs stress are plotted for Berea sandstone in Fig. 8, the maximum strain due to flat crack closing being denoted by a_i(Fig.7). Approximately straight lines result for σ_z vs ε_z and σ_r vs ε_r for both uniaxial compression and hydrostatic compression. The value a_i depends upon orientation of the bedding planes, being approximately 0.84 and 1.67 parallel and perpendicular to the bedding planes of Berea sandstone, and 0.61 and 1.89 parallel

and perpendicular to bedding planes of Ohio sandstone. For Pecos sandstone, this nonlinearity was not observed.

The remarkable characteristic of the final nonlinearity is due to significant volume change. For compression tests the volume change is large for low confining pressure, the circumferential strain being large. On the other hand for higher confining pressure, the stress strain curves approach those for ideal plasticity, the material being incompressible. For extension tests, the volume increase is not affected by confining pressure because expansion of fine cracks. is perpendicular to confining load.

Effect of Pore Pressure

Fig.4 shows an example of the curves of differential stress vs differential strain for various pore pressures. For sandstones used in this work, the curves are essentially the same for $P_o = 0$ and $P_o = 9$ Kpsi. Therefore, the effective stress $\bar{\sigma}_{ij} = \sigma_{ij} + P\delta_{ij}$ holds for the stress-strain relation.

Anisotropy

Bedding planes are visible in Berea and Ohio sandstones but not in Pecos sandstones. The effect of anisotropy on stress strain curves was not observed for Pecos sandstone, but was significant for Ohio and Berea sandstones. The anisotropy was particularly pronounced in the initial nonlinearity, Fig.5 shows clearly the difference between strain parallel and perpendicular to bedding planes. This anisotropy is also observed in tension tests (Fig.6). The slopes are less for specimens with bedding planes perpendicular to the extension load than for those parallel to that load.

In the linear portion of the stress-strain curves, the degree of anisotropy is trivial (Fig.5) In the final nonlinearity, anisotropy is present whether bedding planes are parallel or perpendicular to the axial load; however, due to differences in rock strength parallel and perpendicular to bedding, the nonlinearity starts at lower axial stress in compression tests and at higher axial stress in tension tests for rock specimens with bedding planes parallel to the axial load.

Failure Characteristics

The strength of Berea sandstone is sensitive to confining pressure (Fig.1), increasing significantly with confining pressure for compression tests. On the other hand, for Ohio and Pecos sandstones, the strength does not increase much for confining pressure higher than 3 Kpsi. For extension tests, rock strength is close to that for uniaxial tension tests (Table 1), but it decreases slightly with confining pressure. This may be because, for higher confining pressure, the differential between axial stress and radial stress is large, resulting in yielding of the rock matrix at the edge of microcracks thus lowering tensile strength. It was, however, not observed as previous workers have reported,[7],[14] that tensile strength is significantly reduced by confining pressure so that the sample would split under a stress state of relatively high axial compression.

For compression tests, malleable failure is observed in Pecos and Ohio sandstones as confining pressure increases. At 9 Kpsi confining pressure the strain was so large that stress-strain measurements had to be stopped before fissures appeared. For Berea sandstone no malleable failure was observed, the failure surface being always a single plane. For extension tests no malleable failure was observed, the failure surface being always perpendicular to the axial load.

Table 1 shows experimental results for rock strength. For compression tests on Berea and Pecos sandstone, the effective rock strength was smaller with pore pressure than

without pore pressure. For Ohio sandstone and Indiana Limestone, such difference of strength was not found. For extension test, the effective strength was larger without pore pressure than with pore pressure, except for Indiana limestone which has large variations in strength. Generally, tensile strength of rock is so small that the effects of other factors strengthening the rock are visible. On the other hand, factors for strengthening rock are masked for compression tests because of the large variation of rock strength due to rock heterogeneity. In this experiment, the effective stress constant η for failure, where $\hat{\sigma}_{ij} = \sigma_{ij} + \eta P\delta_{ij}$, is close to 1, being approximately 0.98 for Berea, 0.96 for Ohio and 0.98 for Pecos sandstone in tension tests.

Several workers[7],[14] have reported large effects of pore pressure in limestones and dolomites, although the permeabilities were sufficiently large to inject water. To test this, limestone was used. Since the permeability was around .33 md, nitrogen gas was used as the flowing fluid. In the present experiments, the effect of pore pressure was not observed. Generally these rocks consist of fine pore capillaries and buggy pores. The permeability is governed by fluid flow through large capillaries. Hence, even if the permeability is large, the calculated pore pressure is that of the fluid flowing through these large capillaries but the pressure in the fine capillaries remains unchanged. From the present experiment and those by previous workers one may conclude that η in $\hat{\sigma}_{ij} = \sigma_{ij} + \eta P\delta_{ij}$ is close to 1 if (A) the pressure in all pores is equal and the value is P. ; (B) the rock does not include weak materials which behave like void space.

A THEORY FOR STRESS-STRAIN RELATIONS

Total Stress-Strain Behavior for Sandstone

As shown in the previous section, four portions of the stress-strain behavior with different characteristics were separately expressed by equations in a tensor form and combined to form a total stress strain relation. These four modes are: a linear isotropic part, a nonlinear part caused by pore opening and closing, a plastic part caused by growth of micro-fractures, and a linear isotropic part for interpore materials (Fig.7).

Any system of the total stress σ_{ij} acting simultaneously with a pore pressure P can be divided into two parts: Eq.1 and Eq.2.

$$\bar{\sigma}_{ij} = \bar{\sigma}_{ij} + P\delta_{ij} \qquad \qquad \cdots (1)$$

$$-P\delta_{ij} \qquad \qquad \cdots (2)$$

The strain corresponding to the stress system (Eq.1) is

$$\varepsilon'_{ij} = \frac{1+\nu}{E} \bar{\sigma}_{ij} - \frac{\nu}{E} \delta_{ij} \bar{\sigma}_{kk} + \varepsilon^N_{ij} + \varepsilon^P_{ij}. \qquad \cdots (3)$$

where ε^N_{ij} and ε^P_{ij} are the strains caused by the nonlinear elastic part due to pore opening and closing and the plastic part caused by growth of micro-fractures, respectively.

The strain corresponding to Eq.2 is characterized by the elastic coefficients of interpore materials consisting of interpore matter and nonconnected cracks. Mainly because of the opening, closing, and failure of these cracks, the interpore materials show nonlinearity. On the other hand, since nonlinearity caused by the interpore material is trivial, one may neglect the nonlinear terms, and

$$\varepsilon''_{ij} = - \frac{1-2\nu_i}{E_i} P\delta_{ij} \qquad \qquad \cdots (4)$$

A CONSTITUTIVE EQUATION FOR NONLINEAR STRESS-STRAIN CURVES IN ROCKS AND
ITS APPLICATION TO STRESS ANALYSIS AROUND A BOREHOLE DURING DRILLING

4

SPE 9328

Thus, the total stress-strain relation is

$$\varepsilon_{ij} = \frac{1+\nu}{E} \bar{\sigma}_{ij} - \frac{\nu}{E} \delta_{ij}\bar{\sigma}_{kk} - \frac{1-2\nu_i}{E_i} P\delta_{ij} + \varepsilon_{ij}^N + \varepsilon_{ij}^P \quad \cdots \text{(5)}$$

The details of ε_{ij}^N and ε_{ij}^P will be described in the following sections.

The Stress-Strain Behavior for Nonlinear Part, ε_{ij}^N
_____

Experimental stress-strain measurements showed that sandstones exhibit significant nonlinearity for small load in both compression and extension: (1) the amount of nonlinearity is directional, that is, the strain across the bedding plane is much larger than along the bedding plane; (2) experiments also showed that this nonlinear strain only corresponds to the direction of added stress if the bedding plane coincides with the load. For example, the circumferential nonlinear strain is negligible while the axial nonlinear strain is large for uniaxial compression test; (3) furthermore, ε_{ii}^N vs stress is close to an exponential function approaching a constant value as stress becomes large in the compression side as shown in Fig.7; (4) ε_{ii}^N depends upon $\bar{\sigma}_{ij} = \sigma_{ij} + P\delta_{ij}$. That is, the effect of pore pressure should be subtracted for a rock which has few nonconnected cracks.

The stress-strain relation satisfying all of the above conditions is complicated. For purposes of this work, the function $[\varepsilon_{ij}^N \text{ vs } \bar{\sigma}_{ij}]$ is applied as a first approximation in satisfying the above conditions. This is sufficient for rock of heterogeneous characteristics.

(1) Solve the following equation with respect to the eigen values $\bar{\sigma}$ and the corresponding eigen vectors,

$$(\bar{\sigma}_{ij} - \bar{\sigma}\delta_{ij})\ell_j = 0 \quad \cdots \text{(6)}$$

one obtains the principal stresses $\bar{\sigma}_{ij}'$ and the direction cosines ℓ_{ij}.

(2) The following principal pseudostress is defined corresponding to $\bar{\sigma}_{ij}'$.

$$\tau_{ij}' = (1 - e^{\beta\bar{\sigma}_{ii}'}) \quad \cdots \text{(7)}$$

The form of Eq.7 is obtained from the linearity of the curve $\ln[(a_i - \varepsilon_{ii})/a_i]$ vs effective stress discussed in stress-strain behavior above.

(3) Then the nonlinear strain is given by the anisotropic linear relation with respect to τ_{ij}'.

$$\varepsilon_{ij}^N = a_{im}\tau_{mj} \quad \cdots \text{(8a)}$$

where $\tau_{ij} = \ell_{mi}\ell_{nj}\tau_{mn}' \quad \cdots \text{(8b)}$

The coefficient a_{im} is a tensor of order four and the properties of transformation are followed. Since rock is generally isotropic along the bedding plane, the coefficient a_{ij} is simplified as follows.

$$[a_{ij}] = \begin{bmatrix} a_{11} & a_{12} & a_{13} & & & \\ a_{12} & a_{11} & a_{13} & & 0 & \\ a_{13} & a_{13} & a_{33} & & & \\ & & & a_{44} & & \\ & 0 & & & a_{44} & \\ & & & & & 2(a_{11}-a_{12}) \end{bmatrix} \quad \cdots \text{(9)}$$

, where a_{12} and a_{13} are equal to zero since this nonlinear strain is yielded to the direction of added stress if the bedding plane coincides with the load.

Stress-Strain Relations for Plastic Part, ε_{ij}^P
_____

Stress-strain measurements showed that the rocks exhibit significant nonlinearity before failure occurs. The characteristics of this nonlinearity are as follows: (1) volume change is significant. The rocks always increase in volume in both tension and compression before failure occurs; (2) nonlinearity depends upon the stress level so that one can not apply the deviatoric stress and strain concept; (3) although rocks with bedding planes showed significant anisotropy for small load, they did not show anisotropy after flat cracks in the rocks completely closed; (4) the nonlinearity, before failure, depends mainly upon $\bar{\sigma}_{ij} = \sigma_{ij} + P\delta_{ij}$, that is, the stress added by the pore pressure does not significantly affect it; (5) this nonlinearity is not recoverable and significant hysteresis appears for the unloading process.

After testing various existing plasticity theories, it was found that the kinematic hardening theory could be modified to satisfy the above conditions. An important hypothesis of the kinematic hardening theory is that the plastic strain rate is perpendicular to the yield surface, that is,

$$d\varepsilon_{ij}^P = \lambda \partial f / \partial \bar{\sigma}_{ij} \quad \cdots \text{(10)}$$

where the total stress σ_{ij} is decomposed into $\bar{\sigma}_{ij} = \sigma_{ij} + P\delta_{ij}$ and $-P\delta_{ij}$ and the latter stress is discarded. Note that although hydrostatic stress caused by pore pressure does not significantly contribute to nonlinear strain behavior, that caused by $\bar{\sigma}_{ij}$ is usually non-trivial for rocks.

One may write the deviatoric stress as,

$$S_{ij} = \bar{S}_{ij} + \alpha_{ij} \qquad \ldots(11)$$

where S_{ij} denotes the stress relative to the axis of symmetry and α_{ij} denotes the displacement of the yield surface perpendicular to the hydrostat. The total stress can be written as the sum of three parts

$$\bar{\sigma}_{ij} = \frac{1}{3}\bar{\sigma}_{kk}\delta_{ij} + \alpha_{ij} + \bar{S}_{ij} \qquad ..(12)$$

representing a component along the hydrostat, the displacement of the symmetry, and an increment measured from the symmetry axis, respectively. Since the stress state during yielding stays upon the yield surface, it should satisfy

$$f = 0 \qquad ..(13)$$

where in this work the plastic potential was assumed to have the special form

$$f = \bar{J}_2 - g(\bar{J}_1) \qquad ..(14a)$$

with $\qquad ..(14b)$

$$\bar{J}_1 = \bar{\sigma}_{kk}$$
$$\bar{J}_2 = 3\bar{S}_{kl}\bar{S}_{kl} \qquad ..(14c)$$

For the current application of the kinematic hardening concept, it is assumed that the displacement of the yield surface is proportional to the plastic strain rate, that is,

$$d\alpha_{ij} = b(\bar{\beta})(d\varepsilon^P_{ij} - \frac{1}{3}d\varepsilon^P_{kk}\delta_{ij}) \qquad ..(15a)$$
where
$$\bar{\beta} = \alpha_{1m}\alpha_{1m}/(3\sigma_t + \bar{J}_1) \qquad ..(15b)$$

With this choice of the growth law for α_{ij}, translation of the yield surface is normal to the hydrostat, since

$$d\alpha_{kk} = 0 \qquad ..(16)$$

Substituting Eq.14 into Eq.10 gives

$$d\varepsilon^P_{ij} = \lambda[6\bar{S}_{ij} - g'\delta_{ij}] \qquad ..(17)$$

From both Eqs.15 and 17, one derives

$$d\alpha_{ij} = 6b\lambda\bar{S}_{ij} \qquad ..(18)$$

Multiplying $\bar{S}_{ij}$ on both sides, yields

$$\lambda = \frac{\bar{S}_{kl}d\alpha_{kl}}{2b\bar{J}_2} \qquad ..(19)$$

The final form of the stress-strain relation is

$$d\varepsilon^P_{ij} = \frac{\bar{S}_{kl}d\alpha_{kl}}{2b\,\bar{J}_2}[6\bar{S}_{ij} - g'\delta_{ij}] \qquad ..(20)$$

The function $b(\bar{\sigma}_{kk})$ and $g'(\bar{\sigma}_{kk})$ should be determined by the stress-strain curves measured under triaxial loading.

Range of Stress-Strain Relations

Two definitions of failure are frequently used. One is the point where the rock withstands the maximum load. The other is the point where a definite disruption of rock occurs. The former definition is used in this work for the following reasons. (1) The theory developed in the previous section requires that the crack opening and the crack propagation causing the nonlinearity of rock should exist evenly in the rock from a macroscopic point of view. This condition is normally satisfied up to maximum loading. (2) It simplifies the determination of the kinematic translation b if one uses the stress strain relation in a monotonically increasing region.

Fig.12 shows the strengths of rock under triaxial loading plotted in $\hat{\sigma}_1 \hat{\sigma}_3$ space. It shows that in the tensile region the strengths are approximately constant. In compression region, the curve is close to a parabola for small stresses, while it is close to a straight line for large stresses. From these experimental data and also from the analytical equations by Griffith and Coulomb[9], an approximate curve may be expressed by

$$\hat{\sigma}_3 = \hat{\sigma}_t \qquad \text{for extension} \qquad ..(21a)$$
$$(\hat{\sigma}_1 - \hat{\sigma}_2)^2 + (\hat{\sigma}_3 - \hat{\sigma}_1)^2 \qquad \text{for compression} \qquad ..(21b)$$
where $\qquad + (\hat{\sigma}_1 - \hat{\sigma}_2)^2 = \bar{g}$

$$\bar{g} = \bar{a}_1 + \bar{a}_2(\hat{\sigma}_1 + \hat{\sigma}_2 + \hat{\sigma}_3) + \bar{a}_3(\hat{\sigma}_1 + \hat{\sigma}_2 + \hat{\sigma}_2)^2 \qquad ..(21c)$$

$$\hat{\sigma}_{ij} = \sigma_{ij} + \eta P\delta_{ij} \qquad ..(21d)$$

Eqs.21a and 21b should be applied if all the stress components are either in the tension region or compression region, respectively. However, if some stress components are compressive while others are not, the intersection of these two is often complicated and it is difficult to judge which conditions are to be applied. In order to avoid these situations a reasonable condition should be added to the coefficients of $\bar{g}$. In this work $\bar{g}$ is determined to satisfy the conditions that $\bar{g}$ is a monotonically increasing function and $\bar{g}(3\sigma_t) > 0$ where σ_t is the rock tensile strength. In this situation the failure point can be determined so that failure occurs if one or two conditions given by Eqs. 21a and 21b is satisfied. The lines in Fig. 13 are determined to satisfy the above conditions.

Data Processing

Experimentally it was possible to measure the stress-strain relations under confining pressure without losing accuracy. The equations developed in the previous section are selected so that the triaxial loading equipment is properly applied to them with introducing the effective stress-strain concept. Strictly speaking, polyaxial testing equipment may be

A CONSTITUTIVE EQUATION FOR NONLINEAR STRESS-STRAIN CURVES IN ROCKS AND
ITS APPLICATION TO STRESS ANALYSIS AROUND A BOREHOLE DURING DRILLING

6

SPE 9328

much more realistic for determining better stress-strain relations. The authors, however, feel that polyaxial testing equipment developed so far is not accurate enough to determine more complicated equations and parameters, and thus merely increases the error of stress-strain equations caused by erroneous data. Since the selected equations 14 and 15 include one term on $\overline{J}_1$ and a function $\overline{J}_2$, the intersections between these equations and planes parallel to the π-plane are circles. Accordingly, it provides all the necessary points of stress-strain if one selects loading paths on a certain surface passing through the axis of the loading surface or failure surface, such as loading paths obtained by triaxial loading equipment.

Using programmable loading equipment, empirical data for nonlinear stress-strain were obtained. The necessary data are axial and radial strains, confining and axial stresses. The loading paths consist of tri-axial compression with 3 to 4 confining pressures, triaxial tension with 1 to 2 confining pressures and hydrostatic compression with and without pore pressure. Data are stored on paper tapes. These data in paper tapes are assembled in a file and the coefficients involved in the nonlinear stress-strain equation are determined by appropriate computer programs. Detail fitting of the nonlinear stress-strain equation to experimental data is described in Appendix A. These calculated coefficients are stored in a file to be accessed by simulators.

Due to limited space, only the results on Berea sandstone are mentioned in this paper to show the quality of the constitutive equation. The original porosity was 0.207 and the permeabilities parallel and perpendicular to the bedding plane were approximately 320 md and 260 md, respectively. The empirically measured stress-strain relations are shown in Figs. 1 to 6. These data were numerically processed and ne-cessary coefficients in the nonlinear stress-strain relation were determined. Figs. 9 to 11 show the theoretical nonlinear stress-strain curves. The re-coverability of original data is satisfactory and reflects the characteristics of the original data. More refinement is necessary for small confining pres-sure. For small confining pressure, the yielding mechanism due to internal dislocation is slightly different from those for higher confining pressure. Therefore, the yield surface numerically determined from the empirical stress-strains reflects those for higher confining pressure.

These theoretical curves show that Biot's linear stress-strain relation can be used only for a limited range of stress state. It can not be extended for compression stress states with low confining pres-sure or extension stress states. It also can not be used for stress states higher than two thirds of the maximum strength. In these ranges, the pore fluid pressure causes dislocation of grain contact rather than the continuous deformation assumed by Biot.

FINITE ELEMENT FORMULATION

The equations of equilibrium are

$$\sigma_{ij,j} + F_i = 0 \qquad ..(22)$$

The strain displacement relations are

$$\varepsilon_{ij} = \frac{1}{2}(u_{i,j} + u_{j,i}) \qquad ..(23)$$

The system of Eqs. 5, 13 and 23 give the solution if the pore pressure and boundary conditions are speci-fied. Pore pressure can be given by the diffusivity equation. However, since wall building materials are usually used during drilling and fracture gradient tests, it was assumed to be constant.

The system of nonlinear elasticity equations is reduced to the following formula if one uses the dis-placement approach.[16]

$$K^e\delta^e = F_s^e + F_{\varepsilon^0}^e + F_{\sigma^0}^e + F_p^e \qquad ..(24)$$

where the stiffness matrix and force terms are given as follows

(A) Stiffness matrix

$$K^e = \int_{V^e} [B]^T DB dV \qquad ..(25)$$

In this equation, D and B are elasticity matrix and strain matrix, respectively.

(B) Boundary load

$$F_s^e = \int_S [N]^T t dS \qquad ..(26)$$

where t is the surface load and [N] is the shape function.

(C) The body force caused by the pore pressure

$$F_p^e = \int_{V^e} [B]^T D\varepsilon^P dV \qquad ..(27)$$

where

$$\varepsilon^P = [H]p$$

In this equation, [H] is the strain coefficient matrix caused by the pore pressure.

(D) Force caused by residual strain

$$F_{\varepsilon^0}^e = \int_{V^e} [B]^T D\varepsilon^0 dV \qquad ..(28)$$

(E) Residual stress

$$F_{\sigma^0}^e = -\int_{V^e} [B]^T \sigma^0 dV \qquad ..(29)$$

The shape function used in this work was the two dimensional parabolic isoparametric element shown in Fig. 13. It has eight nodal points in each element and can be used to fit curved boundaries. All the integra-tion appearing in Eqs. 25 to 29 were evaluated with Gauss integration.

There are several nonlinear finite element techniques.[3] These are the initial strain method, the initial stress method and the variable stiffness method. The initial strain method was applied in this

work taking into account its stability and minimum computation time for nonlinear stress strain curves with both concave and convex parts. Modification is possible for the initial strain method. The following initial strain method gave good results.

Let F^e denote the total force except the one due to the residual strain, that is, that

$$F^e = F^e_s + F^e_p + F^e_{\sigma 0} \qquad ..(30)$$

Now the force F^e is devided into M incremental steps.

$$F^e = \sum_{m=1}^{M} \Delta F^m \qquad ..(31)$$

It should be divided along the loading history since the stress-strain depends upon path for plasticity problems. Adding the incremental forces using the following algorithm gives the final stress-strain after M steps.

[Algorithm]

$$
\begin{aligned}
&DO\ m=1,M \\
&DO\ i=1,I \\
&\Delta F^m = \iiint_V [B]^T[D]\{\Delta\epsilon^m_{i-1}\}dv \\
&K\{\Delta\delta^m_i\} = \Delta F^m + \Delta F^m_i \\
&\Delta\sigma^m_i = [D][\{B\}\{\Delta\delta^m_i\} - \Delta\epsilon^m_{i-1}] \\
&\sigma^m = \sum_{\ell=1}^{m-1}\Delta\sigma^\ell + \Delta\sigma^m_i \\
&update \qquad \Delta\epsilon^N + \Delta\epsilon^P \\
&\Delta\epsilon^m_i = .5x[\Delta\epsilon^m_{i-1} + (\Delta\epsilon^N + \Delta\epsilon^P)] \\
&\Delta\epsilon^m = \Delta\epsilon^m_I \quad , \quad \Delta\sigma^m = \Delta\sigma^m_I \\
&\sigma^m = \sum_{j=1}^{m}\Delta\sigma^j, \quad \epsilon^m = \sum_{j=1}^{m}\Delta\epsilon^j + \epsilon^e \\
&\Delta\epsilon^m_0 = \Delta\epsilon^m_I
\end{aligned}
\qquad ..(32)
$$

In this algorithm, the frontal solution with re-solution facility is used to minimize computer time.

APPLICATION OF THE MODEL TO FRACTURE INITIATION DURING DRILLING

Control of drilling fluid leak-off and well kicks during drilling are of great concern to drilling engineers. Drilling fluid loss starts when borehole pressure exceeds the pore pressure for formations with fissures and vuggs. If the wellbore has notches or small fissures, mud loss starts when the wellbore pressure exceeds the least tectonic stress. On the other hand, if the wellbore is smooth, a relatively high pressure is required for breakdown. In this work, this maximum breakdown pressure was calculated to aid the interpretation of leak-off tests and evaluation of fracture gradient.

Assume the formation to be drilled has elastic properties identical to Berea sandstone (i.e., the same stress-strain curves given by Figs. 1 to 6 and a failure surface given by Fig. 12). The overburden stress gradient is assumed to be 1 psi/ft. The horizontal tectonic stress was estimated from the

average horizontal tectonic stress actually measured[2] along the Gulf Coast. Generally, fluid penetration decreases breakdown pressure because the higher pore pressure lowers effective rock strength. Since drilling fluids are wall-building, no allowance was made for breakdown pressure reduction.

Three parameters were varied to study the condition of vertical fracture initiation. These were depth, directional horizontal stress and wellbore shape. Table 2 summarizes the three cases. Case 1 shows the fracture initiation pressure when depth is varied: 7.7 Kpsi for 5000 ft depth; 12.8Kpsi for 10,000 ft; and 17.8 Kpsi for 15,000 ft. Although these values seem to be relatively high, they agree with empirical results, which show high breakdown pressure if the borehole is sealed. The fracture occurs vertically for these cases although borehole pressure exceeds the tectonic stress. This is because the stress state approximates plane strain due to high stress concentrations around the borehole and, consequently, the axial stress is still compressive. It should be noted that the downhole pressure at which formations with preexisting large cracks or fissures will accept whole mud is less than overburden pressure. If fluid penetrates into the formation, the breakdown pressures were lower by numerical simulation model and laboratory experimental tests, i.e., the breakdown pressures calculated by nonlinear simulation models are 5.71 Kpsi, 9.95 Kpsi and 14.2 Kpsi for 5,000, 10,000 and 15,000 ft, respectively, with data given in Table 2 (A,B,C); rock permeability = 320 md; rock porosity = .207; injection fluid compressibility = .155 psi^{-1}; its viscosity = 1cp; and well pressure increasing rate = 1 Kpsi/sec. Also shown are breakdown pressures for linearly elastic material. These results show relatively low breakdown pressure compared with those for nonlinear material; stress concentration is lower for nonlinear material due to relaxation of stresses.

Case 2 is for a slightly higher tectonic stress in one direction. The breakdown pressure is 11.2 kpsi, as compared to 12.8 kpsi for equal horizontal stresses. This results because of tensile stress concentration around the borehole due to the direction of applied loads. An inclined borehole may have the same tendency since the tectonic stress perpendicular to it is directional, although the two stress states would not be identical.

Case 3 is for an elliptic borehole. Actually, a wellbore is rarely circular. Caliper logs often show that the long axis of the elliptic hole is more than 1.5 times larger than the shorter axis. In this case also, the breakdown pressure is lowered.

In the above examples, maximum breakdown pressures are calculated for different parameters. Actual breakdown pressure, however, lies between the following bounds.

$$Min(|\sigma_H|, |\sigma_v|) < P_{actual} < P_b \qquad ..(33)$$

The left hand term is used for designing maximum permissible drilling fluid density. The right hand term is for a wellbore with smooth surface or a surface completely healed by mud cake. During a leak-off test, only a short part of the wellbore is uncased, hence, the probability that fissures or notches exist in this part is small. In this case the actual fracture initiation pressure is close to P_b. It does not, however, mean that all formations below the casing shoe will

A CONSTITUTIVE EQUATION FOR NONLINEAR STRESS-STRAIN CURVES IN ROCKS AND
ITS APPLICATION TO STRESS ANALYSIS AROUND A BOREHOLE DURING DRILLING

8   SPE 9328

hold P_b. It does show that no more than this density mud should be used.

CONCLUSIONS

1. A constitutive equation has been developed which closely fits the nonlinear stress-strain relation of sandstones. Four different phases appear in the stress-strain curves: an initial nonlinear portion, a linear portion, a final nonlinear portion, and the volume change of the rock matrix by pore fluid pressure. The nonlinear strain consists of the sum of these four parts.

2. Precise measurement of the effective stress constant for failure was possible using extension tests, which was not the case for conventional compression techniques owing to rock heterogeneity.

3. Coefficients of the constitutive equation could be determined with reasonable accuracy by simultaneously fitting stress-strain curves for several loading histories in a least square sense. Generally, stress-strain curves are needed for compression tests with 3 to 4 confining pressures, for tension tests with 1 to 2 confining pressures, for hydrostatic compression tests, and for hydrostatic compression with pore pressure equal to confining pressure.

4. A nonlinear stress-strain relation closely fitted to actual rock properties was applied to a finite element model. Its application was feasible although smaller load increments were necessary when the stress state approached rock failure surface.

5. Actual borehole breakdown pressure lies between lower and upper bounds. The lower bound is equal to the smaller value of horizontal or overburden tectonic stress. The upper bound is the breakdown pressure for a smooth wellbore surface. Thus a proper breakdown pressure should be used for preventing or interpreting wellbore problems.

NOMENCLATURE

a_i maximum strain due to the flat crack closing

a_{ij} coefficient tensor for nonlinear stress strain

$\bar{a}_i$ coefficients of the polynomial $\bar{g}$

b function for $d\alpha_{ij}$ vs $d\varepsilon_{ij}^P$

B strain displacement coefficient matrix

D stress strain coefficient matrix

d increment of a variable

E, E_i Young's moduli of the rock and interpore material, respectively

f loading surface

F external force

F_s^e, F_p^e, $F_{\varepsilon^0}^e$, $F_{\sigma^0}^e$ equivalent nodal forces for distributed load, pore pressure, residual strain and initial stress, respectively

F^e total equivalent nodal force

g function for loading surface

$\bar{g}$ function for rock strength

H stress strain coefficient matrix for interpore material

$\bar{J}_1$ $\bar{\sigma}_{kk}$

$\bar{J}_2$ $3\bar{S}_{k\ell}\bar{S}_{k\ell}$

K, K^e stiffness matrix for assembled elements and each element, respectively

ℓ_j, ℓ_{ij} directional cosines

M number of curves

$[N]$ shape function

P fluid pressure

P_c confining pressure

P_o pore pressure

P_{actual}, P_b breakdown pressures for actual and maximum values, respectively

S area

S_{ij} deviatric stress tensor

$\bar{S}_{ij}$ deviatric stress tensor from the axis of the loading surface

t surface load

u_i displacements

V volume

V^e volume of each element

α_{ij} distance between the axis of the loading surface and the hydrostat

β constant

$\bar{\beta}$ variable defined by Eq.15

ε strain

ε_{ij}, ε_{ij}^P, ε_{ij}^N, ε_{ij}^L total, plastic, nonlinear and linear parts of strain tensors, respectively.

ε_{ij}' strain corresponding to the stress system given by Eq.1

ε_{ij}'' strain corresponding to the stress given by Eq.2

δ displacement matrix

δ^e displacement matrix for each element

δ_{ij} Kronecker delta

λ constant

κ $6b\lambda$

γ constant $(0 < \gamma < 1)$

η effective stress constant for failure

ν, ν_m rock and interpore Poisson's ratio

σ stress

σ_{ij} stress tensor

σ^0 residual stress

$\bar{\sigma}_{ij}$ effective stress for stress-strain relation

$\hat{\sigma}_{ij}$ effective stress for failure

$\bar{\sigma}_{ij}'$ effective stress in principal direction

$\bar{\sigma}$ eigen value

σ_t tensile rock strength

σ_H, σ_V horizontal and vertical tectonic stresses, respectively

τ_{ij} pseudostress tensor

τ_{ij}' principal pseudostress

Δ difference between two values

Subscript

i,j indices for tensor components

r, θ space coordinates in radial coordinates

x, z space coordinates in Cartesian coordinates

Superscript

T transpose of a matrix

REFERENCES

1. Barla, G.: "Some Constitutive Equations for Rock Material," Rock Mechanics Theory and Practice (1970) 221.

2. Clark, J.B.: "A Hydraulic Process for Increasing the Productivity of Wells," Trans., AIME, 186, (1949) 1-8.

3. Desai, C.S. and Abel, J.F.: Introduction to the Finite Element Method, Van Nostrand Reinhold. (1972)

4. Dienes, J.K.: "A High-Pressure Kinematic Hardening Model for Rocks and Soils," Jour. Geophy. Res. Vol. 80, (1975) 3749-3754.

5. Drucker, D.C.: "Some Implications of Work Hardening and Ideal Plasticity," Quat. Appl. Math. V7, (1950) 411-418.

6. Drucker, D.C.: "Coulomb Friction, Plasticity, and Limit Loads." Jour. of Appl. Mech., V21, (1954) 71-74.

7. Heard, H.C.: "Transition from Brittle Fracture to Ductile Flow in Solenhofen Limestone as a Function of Temperature, Confining pressure, and Initial Fluid Pressure," Rock Deformation, Geor. Soc. Amer. (1958)193-227.

8. Hill, R.:   The Mathematical Theory of Plasiticity, Oxford University Press, (1960).

9. Mendelson, A.: Plasticity, Macmillan (1968).

10. Morita, N., Kim, C.H. and Gray, K.E.: "Fitting of a Constitutive Equation to the Nonlinear Stress Strain Curves of Sandstones," CESE-DRM-70, (1976).

11. Morita, N. and Gray, K.E.: "Stress State Around a Borehole for a Nonlinear Rock," CESE-DRM-71,(1976).

12. Mroz, A.: "On the Description of Anisotropic Work-hardening," Jour. Mech. Phys. Solids, Vol.15, (1967)163-175.

13. Prevost, J.H., Hughes, T.Jr., and Cohen, M.F." Analysis of Gravity Offshore Structure Foundations," JPT, (Feb. 1980)199-209.

14. Robinson, L.H.Jr.: "The Effect of Pore and Confining Pressure on the Failure Process in Sedimentary Rock," Trans., AIME, 216, (1959)26-32.

15. Sandler, I.S.: "The Cap Model for Static and Dynamic Problems", 17th U.S. Symposium on Rock-mechanics, (1976).

16. Zienkiewicz, O.G.: The Finite Element Method in Engineering Science, McGraw Hill, London.

APPENDIX A

FITTING OF THE NONLINEAR EQUATION TO EXPERIMENTAL DATA

Determination of the linear elastic constants

In Eq.5, all the terms except $(1-2\nu_i)/E_i(P\delta_{ij})$ are functions of $\bar{\sigma}_{ij}$. Hence, if the confining stress and the axial stress are equal to the pore pressure, all the terms vanish except the matrix compression term. Since the bulk modulus of the interpore material is very small, the strain should be measured exactly at balanced pore pressure and confining stress.

Young's modulus and Poisson's ratio should be determined so that the stress-strain relation satisfies the workhardening conditions. From these conditions one derives

$$d\bar{\sigma}_{ij}\,d\varepsilon_{ij} > d\bar{\sigma}_{ij}\,d\varepsilon_{ij}^{L} \qquad (A-1)$$

In addition to this condition, there should exist at least one point which satisfies.

$$d\bar{\sigma}_{ij}\,d\varepsilon_{ij}^{P} = 0 \qquad (A-2)$$

Young's modulus and Poisson's ratio defined above can be calculated from axial and circumferential strain increments and axial and circumferential stress increments at the interval where $\Delta\bar{\sigma}_{ij}\Delta\varepsilon_{ij}$ is maximum.

Actually the measured strain components include the initial and the final portions of nonlinearity. In order to minimize these strains, the linear constants should be evaluated at confining pressure sufficiently high to close flat cracks and at low differential

axial stress before significant yielding appears.

Determination of the coefficients in the initial nonlinear part, ε_{ij}^{N}

Eq.8 includes four components for a_{mn} and one constant β. Since this nonlinear term occurs in the direction of loading, one simple method is to use hydrostatic loading. Usually $a_{11}=a_{22}$, since most rocks are isotropic along the bedding plane. In this case, the specimen with bedding plane perpendicular to the axial load, is loaded hydrostatically, and axial and radial strains are measured until the confining load is high enough that the straight portion appears(Fig. 7). The intersection of the straight portion with the strain coordinate gives a_{11}, a_{22}, and a_{33}. If log $[(\varepsilon_{ii}^{N}+a_i)/a_i]$ vs $\bar{\sigma}_{ii}$ is plotted like Fig.8, the slope gives the value β. The value a_{44} can be determined by a torsion test, but since it is not necessary for plane strain or plane stress problems, it was not measured in this work.

Determination of the functions in the final nonlinear part, ε_{ij}^{P}.

There are several methods to determine these functions. Selection of a proper method determines whether one gets successful results or not. The most important thing to take into account is that the rock is extremely heterogeneous so that the deviation of measured data often exceeds decades of percent, which normal numerical techniques rarely encounter. The methods mentioned in this section are carefully selected so that the resultant stress-strain relation represents the average characteristics of rock samples from a massive rock.

The loading function f which appears in the kinematic hardening theory is similar to the yield surface, and can be determined by yield points. However, for rocks, the final nonlinearity gradually occurs and the yield points are not well defined. In this work, the loading surface is determined so that it passes through points which have specified amounts of nonlinear strain. That is, that

$$f = 0 \text{ for } \varepsilon_{ij}^{P}\varepsilon_{ij}^{P} = \frac{\gamma}{M}\sum_{m=1}^{M}\text{Max}[\varepsilon_{ij}^{P(m)}\varepsilon_{ij}^{P(m)}] \qquad (A-3)$$

The proper value γ may be around 0.02 which is often used to define the yield surface. A polynomial of order 2 was sufficient for the function g in f.

The kinematic hardening function $b(\bar{\beta})$ in Eq.15 is determined from Eqs.14, 16 and 18. These three equations give

$$dS_{ij}^{n+\frac{1}{2}} - d\bar{S}_{ij}^{n+\frac{1}{2}} = d\alpha_{ij}^{n+\frac{1}{2}} \qquad (A-4a)$$

$$6\bar{S}_{ij}^{n+\frac{1}{2}}d\bar{S}_{ij}^{n+\frac{1}{2}} = dg^{n+\frac{1}{2}} \qquad (A-4b)$$

$$d\alpha_{ij}^{n+\frac{1}{2}} = \kappa\bar{S}_{ij}^{n+\frac{1}{2}} \qquad (A-4c)$$

where

$$\kappa = 6b(\bar{\beta})\lambda \qquad (A-4d)$$

$n+\frac{1}{2}$ denotes the value to be evaluated at the center of n-th interval. Eliminating $d\alpha_{ij}^{n+\frac{1}{2}}$ and $S_{ij}^{n+\frac{1}{2}}$ gives

$$\kappa^2 g^{n+\frac{1}{2}} + \left(2g^{n+\frac{1}{2}} + \frac{1}{2}\Delta g^{n+\frac{1}{2}}\right)\kappa + [\Delta g^{n+\frac{1}{2}} \qquad\text{(A-5)}$$

$$-3(2\bar{S}^n_{ij} + dS^{n+\frac{1}{2}}_{ij})dS^{n+\frac{1}{2}}_{ij}] = 0$$

Since all the values except κ can be evaluated for n-th interval if stress strain curves are given, κ can be evaluated at n+½-th point by solving the above equations. From Eqs. A-4a and A-4c, one derives

$$\bar{S}^{n+\frac{1}{2}}_{ij} = \frac{1}{2+\kappa}[2\bar{S}^n_{ij} + dS^{n+\frac{1}{2}}_{ij}] \qquad\text{(A-6)}$$

Using this equation, the deviatoric strain $\bar{S}_{ij}$ can be evaluated for n+½-th point. Finally, substituting Eq.15 into Eq.18 gives

$$b(\bar{\beta})^{n+\frac{1}{2}} = \kappa(g^{n+\frac{1}{2}})/(3\bar{S}^{n+\frac{1}{2}}_{ij} d\varepsilon^{n+\frac{1}{2}}_{ij}) \qquad\text{(A-7)}$$

Thus the function b is evaluated at n+½ th point if stress strain curves are given. Using a polynomial of small degree, $b(\bar{\beta})$ is expressed by $\bar{\beta}$ at all data points in a least square sense.

TABLE 1- EFFECTIVE ROCK STRENGTH

DATA   Bedding Plane : Horizontal for Berea and Ohio
                            Vertical for Pecos and Indiana Limestone
       Pore Fluid   : Water for Berea and Ohio
                             Nitrogen Gas for Pecos and Indiana Limestone

Rock Name	P_c-P_o (Kpsi)	P_o (Kpsi)	$\sigma_{ax}+P_o$ (Kpsi)	Rock Name	P_c-P_o (Kpsi)	P_o (Kpsi)	$\sigma_{ax}+P_o$ (Kpsi)
Extension Tests				Compression Tests			
Berea 15	0.	0.	.14	Berea 1	0.	0.	-9.02
16	0.	0.	.14	2	0.	0.	-9.08
17	0.	0.	.13	33	0.	9.02	-8.63
18	0.	0.	.15				
34	0.	7.01	.30				
Ohio 9	0.	0.	.20	Ohio 1	0.	0.	-6.27
10	0.	0.	.13	2	0.	0.	-5.41
11	0.	0.	.15	3	0.	0.	-6.22
25	0.	6.95	.29	24	0.	9.03	-6.17
26	0.	7.02	.52				
Pecos 8	0.	0.	.57	Pecos 1	0.	0.	-7.59
9	0.	0.	.61	2	0.	0.	-7.42
17	0.	6.98	.69	16	0.	9.02	-6.81
10	-1.02	0.	.17				
18	-1.03	5.96	.61				
11	-3.01	0.	.11				
19	-3.04	3.98	.20				
12	-5.00	0.	.07				
20	-5.03	1.99	.30				
Indiana Limestone				Indiana Limestone			
5	0.	0.	1.50	1	0.	0.	-10.13
6	0.	0.	1.06	2	0.	0.	-14.88
7	0.	0.	.93	3	0.	9.02	-14.42
8	0.	0.	1.30	4	0.	9.04	-13.82
9	0.	6.99	1.12				
10	0.	7.02	1.01				

TABLE 2- MAXIMUM BREAKDOWN PRESSURE FOR VERTICAL FRACTURE

DATA
  (A) Stress-Strain Curves(Figs. 1 to 6)
  (B) Failure Condition (Fig.12)
      Tensile Strength Across the Bedding Plane = .2Kpsi
  (C) Overburden Pressure = 1psi/ft
      Horizontal tectonic stress is estimated from the
      fracture tests in the central and southern area in U.S.A.[2]
      Pore Pressure Gradient = .435psi/ft

CASE 1 Effect of Depth

Depth (ft)	Tec. Stress σ_V (Kpsi)	σ_H	Pore Press. (Kpsi)	Max. Breakdown P Nonlinear (Kpsi)	Linear
5,000	5.	3.95	2.175	7.7	5.93
10,000	10.	7.37	4.35	12.8	10.59
15,000	15.	10.78	6.525	17.8	15.24

CASE 2 Effect of Directional Tectonic Force

Tec. Stress (Kpsi) σ_V	σ_{H1}	σ_{H2}	Pore Press. (Kpsi)	Max. Breakdown P Nonlinear (Kpsi)	Linear
10.	7.37	8.48	4.35	11.2	9.48

CASE 3 Effect of Elliptic Hole($\bar{a}/\bar{b}=2/3$)

Depth (ft)	Tec. Stress σ_V (Kpsi)	σ_H	Pore Press. (Kpsi)	Max. Breakdown P Nonlinear (Kpsi)	Linear
10,000	10.	7.39	4.35	10.35	8.98
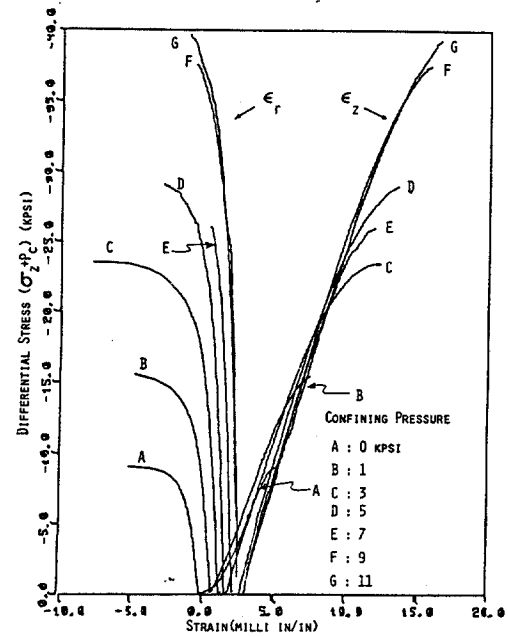
Fig. 1 - Experimental Stress-Strain Curves for
Compression Tests (Berea Sandstone; $P_o=0$;
Horizontal Bedding Plane).
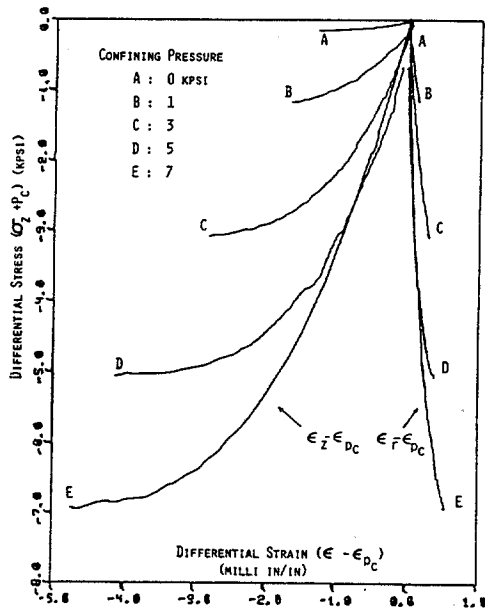
Fig. 2 - Experimental Stress-Strain Curves for
Extension Tests (Berea Sandstone; $P_o=0$;
Horizontal Bedding Plane).
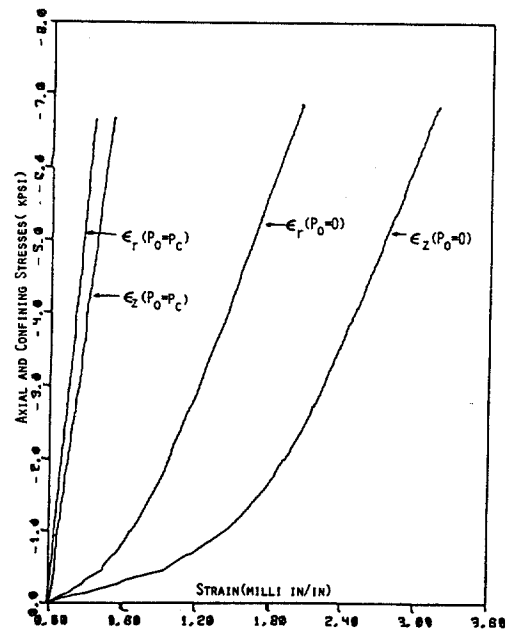
Fig. 3 - Experimental Stress-Strain Curves for
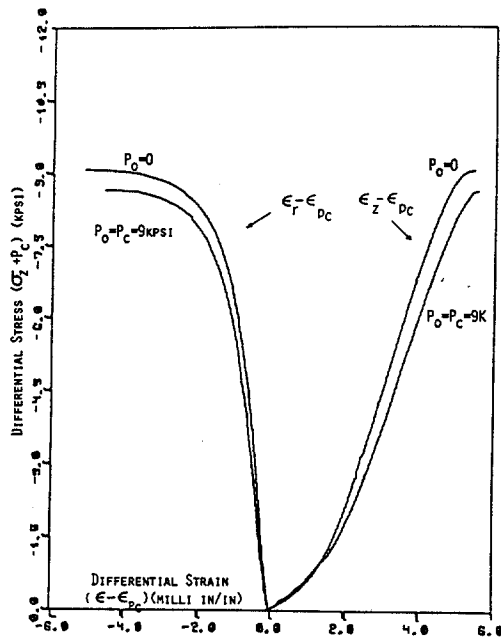Hydrostatic Loading (Berea Sandstone; Horizontal
Bedding Plane).

Fig. 4 - Experimental Stress-Strain Curves with and without Pore Pressure (Berea Sandstone; Horizontal Bedding Plane).
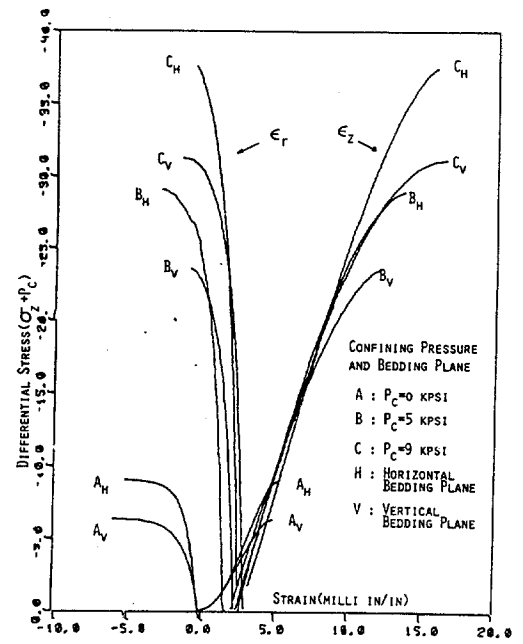

Fig. 5 - Experimental Stress-Strain Curves for Specimen with Horizontal and Vertical Bedding Plane (Compression; Berea Sandstone; $P_o=0$).
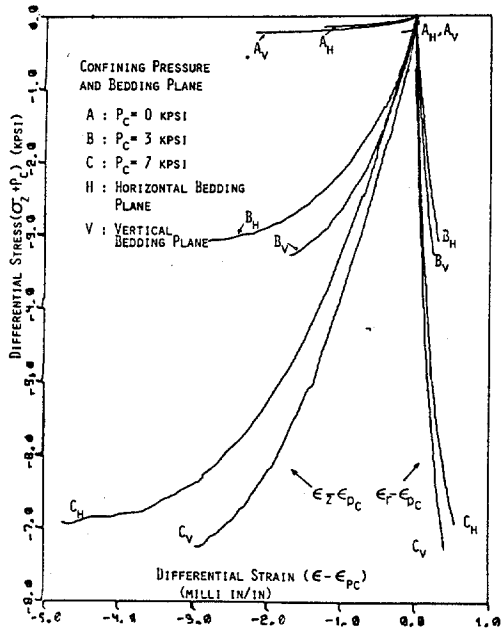

Fig. 6 - Experimental Stress-Strain Curves for Specimen with Horizontal and Vertical Bedding Plane (Extension; Berea Sandstone; $P_o=0$).
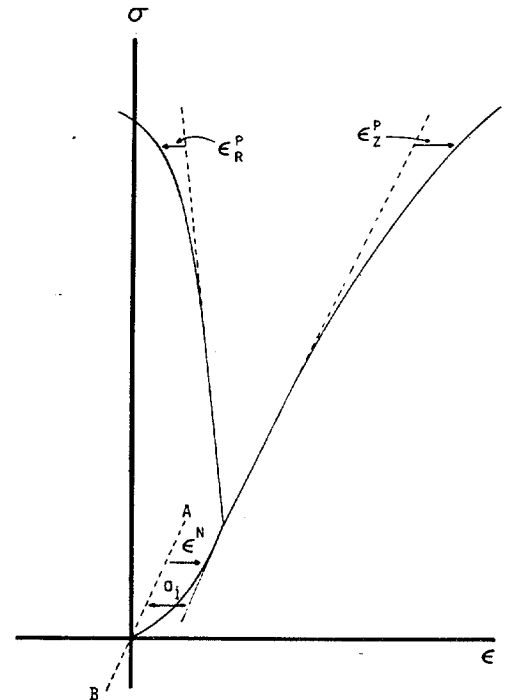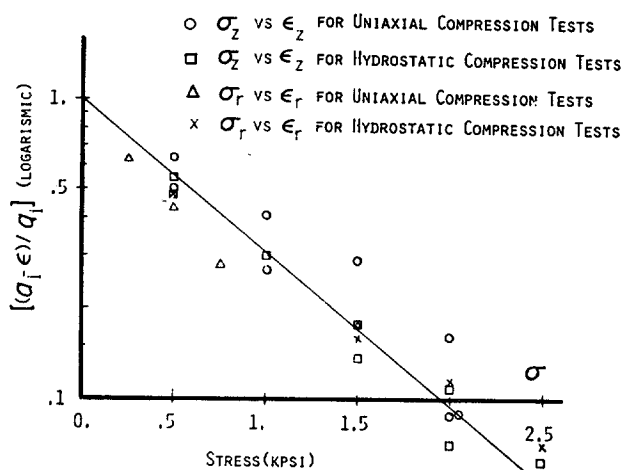

Fig. 7 - Schematic Diagram for Initial and Final Portions of Nonlinearity.

Fig. 8 - Initial Nonlinear Stress-Strain (Berea).
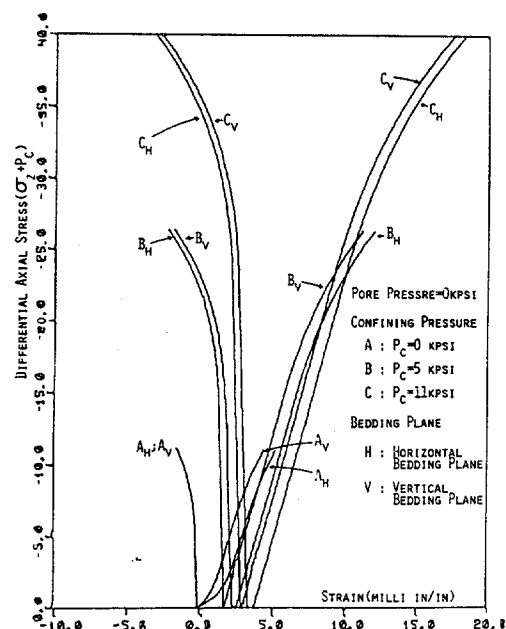
Fig. 9 - Theoretical Stress-Strain Curves for Compression Loading (Berea Sandstone; Horizontal and Vertical Bedding Planes; $P_o = C$).
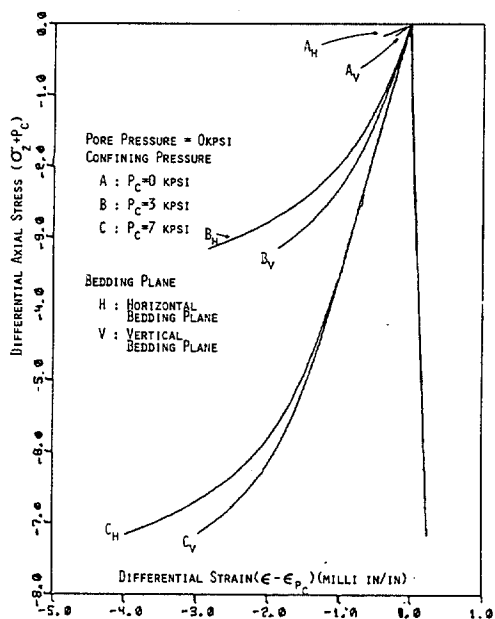

Fig. 10 - Theoretical Stress-Strain Curves for Extension Loading (Berea Sandstone; Horizontal and Vertical Bedding Planes; $P_o = 0$).
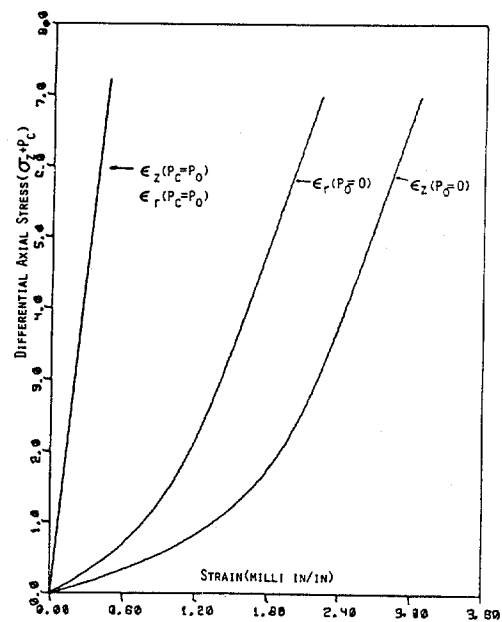

Fig. 11 - Theoretical Stress-Strain Curves for Hydrostatic Loading (Berea Sandstone; Horizontal Bedding Plane).

$$\vec{G} = \bar{A}_1 + \bar{A}_2 J + \bar{A}_3 J^2$$

WHERE $\bar{A}_1 = 6.9563$
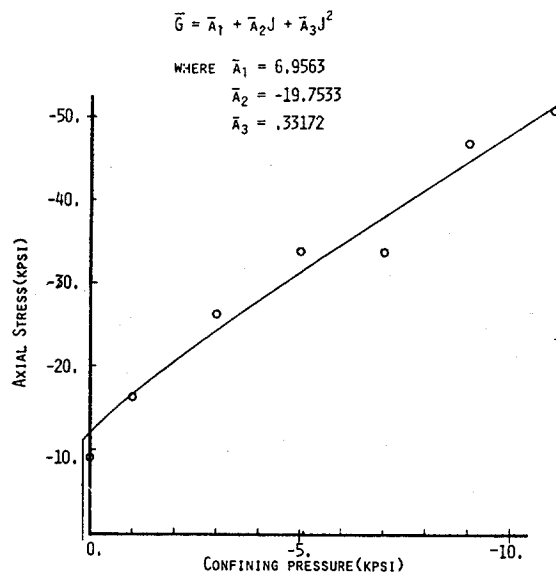$\bar{A}_2 = -19.7533$
$\bar{A}_3 = .33172$

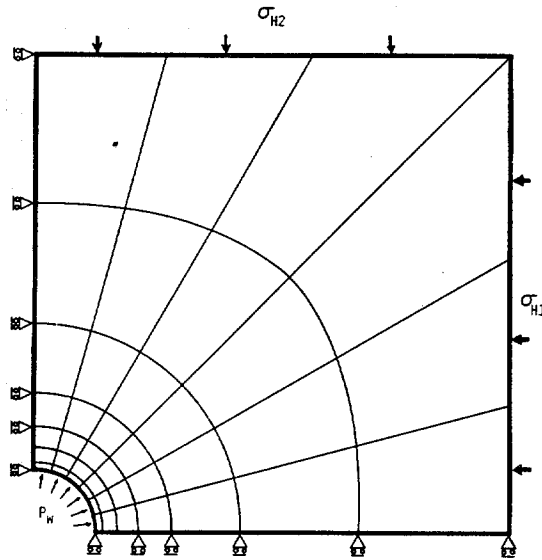Fig. 12 - Failure Envelope for Berea Sandstone.

Fig. 13 - Finite Element Idealization Around a
Borehole Using the Parabolic Isoparametric
Element.